Eddy-wall encounters: decay, squeeze, image effect, and their strange dependence on the boundary conditions

09/20/12

Volodymyr Zharkov[1], Doron Nof[2,3], Alexandra Bozec[1], Wilton Arruda[2,4], and Eric Chassignet[1]

1. Center for Ocean-Atmospheric Prediction Studies, Florida State University, Tallahassee, Florida 32306, USA
2. Department of Earth, Oceans and Atmospheric Science, Florida State University, Tallahassee, Florida 32306, USA
3. Geophysical Fluid Dynamics Institute, Florida State University, Tallahassee, Florida 32306, USA
4. Instituto de Matemática, Universidade Federal do Rio de Janeiro (UFRJ), Rio de Janeiro, RJ, Brazil.

Abstract

The encounters of westward propagating baroclinic eddies with a meridional wall on a β-plane and on an f-plane are considered both analytically and numerically using a reduced gravity model. It is shown that the eddy–wall interaction dramatically depends on the type of boundary conditions at the wall. On a β-plane, in the case of the no-slip boundary condition, no image effect occurs, so the eddy remains tangent to the wall and does not propagate in the meridional direction. Its radius diminishes gradually because of leakage at a rate that varies from $1/\left\{1+\alpha\beta R_0 t/\left[12(2\alpha+1)\right]\right\}$ for lenses to $1/\left(\beta R_0 t/8\right)$ for deep upper layer eddies, where α is the vorticity coefficient. In the case of a free-slip condition, a non-lens eddy squeezes onto the wall, and a strong image effect occurs, pushing the eddy poleward. An equation defining the squeezing coefficient δ (i.e. ratio of the width of the squeezed segment to the eddy radius) as a function of time is obtained. The eddy propagation rate along the wall due to the image effect is expressed in terms of δ.

On an f-plane, numerical simulations show that a non-lens eddy initially tangent to a slippery wall also squeezes and is subjected to the image effect (mostly because of alteration due to the viscosity in numerics). It translates along the walls of the rectangular domain with a propagation speed that can be roughly estimated using the formula obtained for encountering eddies on a β-plane. In the case of a no-slip wall condition, the eddy stays tangent to the wall at the same location and gradually dissipates.

1. Introduction

The eddy–wall interaction problem is not new. In fact, it has been studied from many different points of view. Lamb (1932), Saffman (1979), Pierrehumbert (1980), Minato (1982, 1983), Wu et al. (1984), Umatani and Yamagata (1987), and Masuda (1988) worked with linear quasigeostrophic eddies and with encounters taking place on an f-plane. Yasuda et al. (1986) were among the first to consider interaction on a β-plane. Nof (1988a) proposed an analytical modeling approach for eddy–wall interactions, considering a barotropic eddy with a small Rossby number, where interactions took place on an f-plane. He concluded that an anticyclonic (cyclonic) eddy encountering a zonal boundary leaks interior fluid from its right (left) side, looking offshore, after the contact. Nof (1988b) considered the interaction involving two types of baroclinic eddies: quasigeostrophic linear and moderately nonlinear. The former showed the same behavior as the barotropic eddies in Nof (1988a). For the later, however, there was no leak along the wall. The author explained this unexpected absence as a result of the high inertia of fluid particles inside the eddy.

Shi and Nof (1993) investigated a violent encounter of an eddy with a meridional wall on an f-plane, resulting in a massive leak from the eddy interior and the subsequent split of the eddy. In this case, the collision of a cyclonic (anticyclonic) eddy with a wall produces an offspring anticyclonic (cyclonic) eddy, with the anticyclonic feature on the left side of the contact zone. The eddies move away from each other because of the image effect.

Shi and Nof (1994) investigated soft eddy–wall interactions on a β-plane, where three factors influence along-wall migration of the eddy: the image effect [see Lamb (1932), Kundu and Cohen (2008) for its explanation in a hydrodynamic sense], the β-induced force, and the "rocket" force (due to the momentum of the leaking fluid). Also, these authors considered interactions between non-lens quasigeostrophic eddies and a wall on an f-plane. After contact, the eddy assumes a semicircular shape (which they called a "wodon") that has a structure entirely different from that of an eddy in the open ocean. The wodons do not show leaks, leading to the conclusion that, for eddies with low Rossby numbers, the leaks do not have an important role in the interaction. The importance of the leakage increases proportionally with the nonlinearities of the eddy itself.

Zavala Sansón et al. (1998) and Nof (1999) investigated encounters between anticyclonic lens-like eddies and a wall on a β-plane. Again the balance of forces along the wall involved three processes: the Coriolis force, the β-induced force, and the rocket force. The image effect was assumed negligible because, for lenses, the area of eddy–wall contact is very small. Zavala Sansón et al. (1998) showed that the lenses leak fluid while keeping their circular shape. The initial direction of their meridional migration depends on the relationship between their potential vorticity (PV) and the β-effect but, finally, the eddy migrates equatorward. Nof (1999) obtained an analytical formula for eddy decaying, in agreement with the results of Zavala Sansón et al. (1998). The equatorward translation of lenses is, however, very weak according to Nof (1999). In the author's point of view, the results could not be extended to non-lenses because the image effect could be significant, and it is not quite clear how to account for the effect in the force balance approach.

As Shi and Nof (1994) and Azevedo et al. (2012, in press) suggested, eddy–continent interactions due to β are relatively "soft" because the eddy translation speed is very small [$\sim O(\beta R_d^2)$, where R_d is the eddy Rossby radius]. We note, however, that there are eddy–continent interaction cases, where the eddy structure is dramatically altered within a few days (e.g., Shi and Nof, 1993).

In this paper, we show that, for non-lenses, the image effect is negligible for a no-slip boundary condition (NSBC). In contrast, in the case of a free-slip boundary condition (FSBC), the image effect is significant and leads to the propagation of the eddy along the wall. We suggest a formula for the propagation velocity owing to the image effect and show that the balance between the three other effects (considered by Nof, 1999) is still responsible for estimating the eddy radius decreasing rate and the amount of leakage. Also, in this paper we will show that a "viscous" image effect appears even in the *f*-plane simulations for an eddy initially tangent to the wall. We will suggest a possible explanation for this effect.

The paper is organized as follows. In Section 2, we discuss the governing equations for the eddy-wall encounters on the β-plane. In Section 3, we present the numerical runs in different scenarios of encounters depending on the boundary conditions. In Section 4, we describe the equations for the evolution of an eddy during the encounter and its propagation due to the image effect (a detailed development of the equations is given in Appendix A). Section 5 is devoted to the consideration of the viscous image effect on an *f*-plane. Finally, we summarize our results in Section 6. For convenience, we list all the relevant symbols in Appendix B.

2. Formulation

In this section, we consider the equations governing an eddy's (not necessarily a lens's) encounter with a vertical meridional wall (at $t = 0$) as a result of β-induced westward propagation. A simple one-and-half-layer model is used, where an active upper layer (with density ρ) is atop an infinitely deep stagnant layer with density $(\rho + \Delta\rho)$. At this time we, at least formally, do not take into account the image effect, which will be discussed later. The basic approach and the scale analysis are similar to those given in Nof (1999).

A schematic diagram of the model is shown in Figure 1. As the eddy is pushed against the wall, it leaks, and its volume decreases gradually. Later (in Section 4), we will consider two scenarios of eddy–wall interaction and the possibility of along-wall propagation. In both cases, we deal with two time scales. The first is a "fast" scale of $O\left(|f|^{-1}\right)$ characterizing the geostrophic adjustment and period of particle rotation inside a zero vorticity eddy, where *f* is the Coriolis parameter. The second is a "slow" scale of $O(\beta R_d)^{-1}$ that characterizes the eddy drift toward the wall. Here R_d is the Rossby radius of the eddy, and β the meridional gradient of *f*. Assuming that the parameter $\varepsilon = \beta R_d / |f|$ is small, we will analyze the scales in the following equations.

a. Conservation of mass.

We assume that the decrease of the eddy volume is due to leakage, and that the leakage velocity v is constant over its cross section (and equals the eddy orbital velocity along its rim, according to Bernoulli principle). We calculate the leakage transport across the segment PP_1 (Fig. 1) by integrating $v\left[H+\tilde{h}(x,t)\right]$ over this segment, where H is the undisturbed upper-layer depth outside the eddy, and $\tilde{h}$ is the perturbation depth. As the leakage is assumed approximately geostrophic in the cross-stream direction, its width is $l=\left|g'h^*\left(f_0v\right)^{-1}\right|$ (where $v<0$ for anticyclonic eddies), g' is the reduced gravity, f_0 is the absolute value of the Coriolis parameter at the eddy center, and $h^*=h^*(t)=\tilde{h}(0,t)$. As a result, the mass conservation equation is

$$\frac{dV}{dt}=-\frac{g'}{f_0}\left(Hh^*+\frac{h^{*2}}{2}\right), \tag{1}$$

where V is the eddy volume. As we assume that V slowly varies in time, the left-hand side of (1) has a scale $\varepsilon f^3R_d^4/g'=\varepsilon g'H_e^2/f$ where H_e is the characteristic depth of the eddy (i.e., the depth of the upper layer at the eddy center.) Therefore, the scale of h^* varies from $\varepsilon^{1/2}H_e$ for lenses ($H=0$) to εH_e for non-lenses (when H is comparable to H_e). Accordingly, the scale of l is $\varepsilon^{1/2}R_d$ for lenses (Nof, 1999) and εR_d for non-lenses.

b. Momentum flux.

In a coordinate system moving with the eddy center, the nonlinear momentum equations (multiplied by the upper-layer depth h) and continuity equation are

$$h\frac{\partial u}{\partial t}+h\frac{\partial C}{\partial t}+hu\frac{\partial u}{\partial x}+hv\frac{\partial u}{\partial y}-\left(f_0+\beta y\right)vh+\frac{g'}{2}\frac{\partial}{\partial x}\left(h^2\right)=0, \tag{2a}$$

$$h\frac{\partial v}{\partial t}+hu\frac{\partial v}{\partial x}+hv\frac{\partial v}{\partial y}+\left(f_0+\beta y\right)\left(u+C\right)h+\frac{g'}{2}\frac{\partial}{\partial y}\left(h^2\right)=0, \tag{2b}$$

$$\frac{\partial h}{\partial t}+\frac{\partial}{\partial x}\left(hu\right)+\frac{\partial}{\partial y}\left(hv\right)=0, \tag{3}$$

where $C(t)$ is the eddy zonal propagation speed, h is the depth of the upper disturbed layer ($h=H$ far away from the currents and BE), and $g'=g\Delta\rho/\rho$ is the reduced gravity. In this coordinate system, the wall is "moving toward the eddy," so the boundary condition at the wall is

$$u=-C \text{ at } x=x_{wall}-\int_0^t C\,dt\,.$$

As a significant simplification of our model, we assume that the eddy *acceleration* in the meridional direction is small, at least for a while, so that its along-wall propagation speed, if nonzero, is almost constant, and we can consider the system of equation solely in the zonal direction. Hence, we add (2b) and (3) multiplied by v, and integrate along the contour *PQRS* (Fig. 1 here). As a result, we obtain the basic momentum equation

$$\begin{aligned}\iint_S h\frac{\partial v}{\partial t}dS+\iint_S v\frac{\partial h}{\partial t}dS+\iint_S\left[\frac{\partial}{\partial x}\left(huv\right)+\frac{\partial}{\partial y}\left(hv^2\right)\right]dS+\iint_S\left(f_0+\beta y\right)uhdS\\ +\iint_S\left(f_0+\beta y\right)ChdS+\frac{g'}{2}\iint_S\frac{\partial}{\partial y}\left(h^2\right)dS=0,\end{aligned} \tag{4}$$

which is analogous to (2.4) in Nof (1999). Here S is the area enclosed by *PQRS*.

Following Nof's (1999) scaling, we drop the terms smaller than $O(\varepsilon)$. First, we note that v can be considered as $(\bar{v}+v')$, where $\bar{v}$ is the meridional speed in absence of a wall, and v' is the time-dependent disturbance (due to the wall approaching) whose scale is $O\left[(\varepsilon g'H_e)^{1/2}\right]$. Therefore, under our assumption of slow variations, the time scale of the $h\partial v/\partial t$ inside the eddy is $O\left[\varepsilon^{3/2}(g'H_e)^{1/2}fH_e\right]$. Less obvious is the order of the second term. Here, the integrand is $O\left[\varepsilon(g'H_e)^{1/2}fH_e\right]$. For lenses, Nof (1999) argued that the contribution to the integral is from the asymmetrical part of v only, so the order of the integral is not more than $O\left[\varepsilon^{3/2}(g'H_e)^{1/2}fH_eR_d^2\right]$. In our case, the significant deformation of the eddy shape due to the wall is allowed, so the asymmetry of velocities is essential. However, we assume that: (i) the speed of the wall "intrusion" into the eddy is $O\left[\varepsilon(g'H_e)^{1/2}\right]$, and (ii) the eddy keeps its circulation, so, according to the mass conservation, $\iint_S v\,dS \sim O\left[\varepsilon(g'H_e)^{1/2}R_d^2\right]$. On the basis on these assumptions, we conclude that the contribution from the eddy area to the second term in (4) is $O\left[\varepsilon^{3/2}(g'H_e)^{1/2}fH_eR_d^2\right]$ as well. Finally, the contribution from the leakage in the two first terms (with time derivatives) of (4) is also negligible because the leakage area is small.

Let the streamfunction ψ be $\partial\psi/\partial y=-uh;\ \partial\psi/\partial x=vh$. From Stokes' theorem, it follows from (4) that

$$-\oint_{\partial S} hv^2\,dx+\oint_{\partial S} huv\,dy-\iint_S f_0\psi_y\,dS-\beta\iint_S y\psi_y\,dS+C(t)\iint_S (f_0+\beta y)h\,dS \\ -\frac{g'}{2}\oint_{\partial S} h^2\,dx=0, \qquad (5)$$

where ∂S is the boundary of the region S (Fig. 1). The second term is zero (because at least one of the three multipliers of the integrand vanishes at each part of the integration contour), and, after integrating the fourth term by parts, we rewrite (5) as

$$\oint_{\partial S}\left(-hv^2 + f\psi - \frac{g'}{2}h^2\right)dx + \beta\iint_S \psi\, dS + C(t)\iint_S \left(f_0 + \beta y\right)h\, dS = 0. \tag{6}$$

Further simplifications are made neglecting small terms as described in Appendix A. We finally obtain

$$-\int_P^{P_1} hv^2\, dl + \beta\iint_{S_e}\psi\, dS + C(t) f_0 V_b = 0. \tag{7}$$

Here, $V_b = \iint_{S_e}\tilde{h}\, dS$ is the volume of the eddy "bell" (see schematic Fig. 2), whose depth is $\tilde{h}(r) = h - H$, and S_e is the eddy area. Note that $\tilde{h}$ is *negative* for cyclones.

Under the same assumptions that led to (1) (i.e., the BE volume decreases owing to the leakage, which is approximately geostrophic, and the leakage velocity is almost constant over the width), the first term in (7) is $-v\int_P^{P_1} hv\, dl = -v\, dV/dt$, implying that v is the velocity of leakage here. So, according to the Bernoulli principle, (7) takes the form

$$-v_\theta(R)\frac{dV}{dt} + \beta\iint_{S_e}\psi\, dS + C(t) f_0 V_b = 0, \tag{8}$$

where

$$v_\theta = -\alpha f_0 r/2, \quad r \le R \tag{9}$$

is the eddy orbital velocity, and α is twice the eddy Rossby number ($\alpha = 1$ for zero PV eddies.) Though the simplifications used to obtain (8) are justifiable, this equation still neglects the image effect. Since it is not easy to consider this effect theoretically, numerical experiments are performed to better understand its role. We describe our numerical set-up in the next section.

3. Numerical experiments on a β-plane.

A modified version of the Bleck and Boudra (1986) reduced gravity isopycnic model with a passive lower is used. The basin size is taken to be 1600×1600 km; the horizontal resolution is 5 km, and the time step is 30 s. The parameters are $g' = 2 \times 10^{-2}$ m s^{-2}, $f_0 = 8.8 \times 10^{-5}$ s^{-1}, $\beta = 2.3 \times 10^{-11}$ m^{-1} s^{-1}, $R = 50$ (or 100) km, $H = 300$ (or 500) m, and initially $\alpha = 1$. During the experiments, the value of α is altered by the viscosity effect, as discussed in Zharkov and Nof (2008b).

We start the experiments at $t = 0$ by turning on a circular anticyclonic eddy centered at a point whose distance from the wall is twice the eddy radius, and run for 720 days. The results presented here are for R = 100 km and $H = 500$ m. The viscosity coefficient ν is taken to be 350 m^2 s^{-1}, which is the minimum required for numerical stability (in this case, the diffusion speed is 0.07 m s^{-1}, which is small compared to the eddies orbital speed of at least 1 m s^{-1}). Figure 3 shows the evolution of the eddy during the first 80 days of simulation for NSBC (left panel) and FSBC (right panel). The behavior of the eddy differs between the two cases. With NSBC, the eddy remains tangent to the wall at all times, and its radius monotonically decreases, probably because of the leakage. The tangency point between the eddy and the wall slightly shifts along the wall during the simulation. This behavior is similar to the behavior of a lens (Nof, 1999), justifying the neglect of the image effect in (8). In contrast, with FSBC, a nearly wodon scenario occurs: the eddy squeezes against the wall, deforms significantly, and moves poleward along the wall because of the image effect, as will be described in the next sections. However, because (i) the center of the eddy moves towards the wall at approximately the same rate in both cases, and (ii) (8) (defining the movement of the eddy in zonal direction) is obtained disregarding the boundary conditions, we will consider the two different scenarios: a tangent scenario and a "wodonization" scenario. For both, we consider that, at least at the first stage of the eddy–wall interaction, the decay and squeezing of the eddy can be essentially described by (8), so that the image effect is responsible exclusively for the eddy along-wall propagation.

4. Theoretical description of the eddy–wall interaction

a. Tangent scenario

On the basis of our numerics, we assume that the eddy is circular (i.e., distortions caused by both the β-effect and the intrusion of the wall are of the next order of smallness). Under NSBC, we generalize the formulas given in Nof (1999). Assuming that the eddy is radially symmetric (in a polar coordinate system with origin at its center), we have

$$\frac{v_\theta^2}{r} + f_0 v_\theta = g'\frac{\partial h}{\partial r}, \tag{10}$$

where v_θ is defined by (9). Since $h = H$ at the eddy rim ($r = R$), we obtain

$$h(r)=\tilde{h}(r)+H,\ \tilde{h}(r)=\frac{\alpha(2-\alpha)f_0^2}{8g'}\left(R^2-r^2\right). \tag{11}$$

Assuming that the eddy remains approximately circular, its volume is $2\pi\int_0^R h(r)r\,dr$, and

$$V=V_b+\pi R^2 H;\quad V_b=\frac{\pi\alpha(2-\alpha)f_0^2R^4}{16g'}. \tag{12}$$

Also, for radially symmetric eddies (see Nof, 1981), $\psi=-\int_r^R v_\theta h\,dr$, and

$$\beta\iint_{S_e}\psi\,dS=2\pi\int_0^R r|\psi|dr=\frac{\pi\alpha\beta f_0R^4}{8}\left[\frac{\alpha(2-\alpha)f_0^2R^2}{24g'}+H\right]. \tag{13}$$

Substituting (12) and (13) into (8) with $C(t)=dR/dt$, we obtain the differential equation for the time-evolution of the eddy radius

$$\frac{dR}{dt}=-\frac{\beta R^2}{12}\frac{\alpha(2-\alpha)f_0^2R^2+24g'H}{(2-\alpha)(2\alpha+1)f_0^2R^2+16g'H}. \tag{14}$$

If we assume that the initial moment of time is zero, for anticyclonic eddies ($0<\alpha\le 1$), the solution of (14) is

$$t=\frac{4}{\beta}\left[\frac{2}{R}-\frac{(4\alpha+3)f_0}{2}\sqrt{\frac{2-\alpha}{6\alpha g'H}}\tan^{-1}\left(\frac{f_0R}{2}\sqrt{\frac{\alpha(2-\alpha)}{6g'H}}\right)\right]\Bigg|_{R_0}^{R}, \tag{15}$$

where $R_0=R(0)$.

In this work, we assume that cyclonic eddies ($\alpha<0$) never outcrop, i.e., $h(r)>0$ everywhere. According to (11), the non-outcropping criterion is

$$\frac{\alpha(2-\alpha)f_0^2R^2}{8g'}+H>0\Rightarrow\sqrt{8g'H}>\sqrt{\alpha(\alpha-2)}f_0R. \tag{16}$$

In this case, the solution of (14) is

$$t=\frac{4}{\beta}\left[\frac{2}{R}-\frac{(4\alpha+3)f_0}{4}\sqrt{\frac{\alpha-2}{6\alpha g'H}}\log\left(\frac{2\sqrt{6g'H}+\sqrt{\alpha(\alpha-2)}f_0R}{2\sqrt{6g'H}-\sqrt{\alpha(\alpha-2)}f_0R}\right)\right], \tag{17}$$

where $\left(2\sqrt{6g'H}-\sqrt{\alpha(\alpha-2)}f_0R\right)>0$ due to (16).

In the case of lenses ($H=0$), (14) is reduced to

$$\frac{dR}{dt}=-\frac{\alpha\beta R^2}{12(2\alpha+1)}. \tag{18}$$

So, the solution is

$$R=R_0\left[1+\frac{\alpha\beta R_0 t}{12(2\alpha+1)}\right]^{-1}. \tag{19}$$

For zero PV ($\alpha=1$), this equation takes the form of (3.7) from Nof (1999).

In the opposite limit $H\rightarrow\infty$, called a cylindrical eddy (when the Rossby radius of the upper-layer depth is much larger than the eddy radius), we have

$$\frac{dR}{dt}=-\frac{\beta R^2}{8}. \tag{20}$$

The solution is

$$R=R_0\left(1+\frac{\beta R_0 t}{8}\right)^{-1}. \tag{21}$$

For $R_0=50$ km and $\alpha=\pm 1$, the evolution of the eddy radius modeled by (14) and the respective volume for the different kinds of eddies is shown in Figure 4. It can be seen that the non-lenses (and especially cyclones) decay much faster at the beginning of the squeezing process than the lenses do. This can be explained by the fact that initially the contact area between the wall and a lens is very small, so the encounter is much softer than for a non-lens eddy. However, the decaying process slows with time. The transition from a lens to a cylindrical eddy occurs quickly with growing H (the "intermediate" case is $H = 50$ m, yellow line in Fig. 4a). If H is of the order of the bell depth (which is about 125 m for $R = 50$ km and $\alpha = 1$), the evolution of the radius is similar to the cylindrical eddy. Similar conclusions can be drawn for $H = 500$ m. Consequently, the difference in decaying between cyclonic and anticyclonic eddies of the same H is small (see blue and green lines for $H = 500$ m, and magenta lines for $H \to \infty$ in Fig. 4a). At the same time, the decrease in volume (Fig. 4b) for an anticyclonic eddy with $H = 500$ m (blue line) is similar to the decrease of the cylindrical eddy volume (magenta line) but is significantly different from that of a cyclonic eddy (green line).

b. Wodonization scenario

Now, we return to the situation depicted in Figure 1 and assume that, as the eddy is pushed against the wall, it deforms into a wodon. At the same time, the eddy propagates along the wall because of the image effect (which will be considered below), so we assume (8) to be valid in a coordinate system moving with the eddy center along the *y*-axis. The distortion due to the interaction with the wall is $O(1)$ but we assume that at least with error of $O(\varepsilon^{1/2})$, the purely *geometrical* description of the wall intrusion can be used. As before, any distortions due to β are neglected. In this case, the (darker) region *ACB* (Fig. 1) gradually enlarges, and the remaining area S_e decreases as a function of *t*. The integration in the second and third terms of (7) is carried out over $S_e(t)$. If the length of *CD* is *b*, then *OD* length is $R-b$ and the *BD* length is $\sqrt{b(2R-b)}$. The value (in radians) of the angle φ is $2\cos^{-1}(1-\delta)=2\sin^{-1}\sqrt{\delta(2-\delta)}$, where $\delta=b/R$. Therefore, the area of the region S_e is

$$\begin{gathered}\iint_{S_e(t)} dS = I_1(R,\delta)=\pi R^2 G_1(\delta),\\ G_1(\delta)=1-\frac{1}{\pi}\left[\sin^{-1}\sqrt{\delta(2-\delta)}-(1-\delta)\sqrt{\delta(2-\delta)}\right].\end{gathered} \tag{22}$$

If the eddy evolves completely into a wodon, the final value of *b* is *R* (i.e., $\delta=1$). We assume that $C(t)=-db/dt=-R\,d\delta/dt$. The *initial* expressions for the second term in (8) and V_b are (13) and (12), respectively. However, during the wodonization process ($t>0$),

$$V_b=\frac{\alpha(2-\alpha)f_0^2}{8g'}I_2, \tag{23}$$

$$\beta\iint_{S_e(t)}|\psi|dS=\frac{\alpha\beta f_0}{4}\left[\frac{\alpha(2-\alpha)f_0^2}{16g'}I_3+I_2H\right], \tag{24}$$

where $I_2(R,\delta)=\iint_{S_e(t)}\left(R^2-r^2\right)dS$ and $I_3(R,\delta)=\iint_{S_e(t)}\left(R^2-r^2\right)^2 dS$.

Calculating the double integrals, we obtain

$$\begin{gathered}I_2(R,\delta)=\frac{\pi R^4}{2}G_2(\delta),\\ G_2(\delta)=1-\frac{1}{\pi}\left[\sin^{-1}\sqrt{\delta(2-\delta)}-\frac{\sqrt{\delta(2-\delta)}(1-\delta)\left(3+4\delta-2\delta^2\right)}{3}\right];\end{gathered} \tag{25}$$

and

$$I_3(R,\delta) = \frac{\pi R^6}{3} G_3(\delta),$$
$$G_3(\delta) = 1 - \frac{1}{\pi}\left[\sin^{-1}\sqrt{\delta(2-\delta)} - \frac{\sqrt{\delta(2-\delta)}(1-\delta)\left(15+20\delta+22\delta^2-32\delta^3+8\delta^4\right)}{15}\right]. \tag{26}$$

The functions $G_i(\delta)$ ($i = 1, 2, 3$) are plotted in Figure 5. Initially, the eddy is tangent to the wall, so that $G_1(0) = G_2(0) = G_3(0) = 1$, and we recover (12)–(13) from (22)–(24). At the initial stage of the squeezing process, G_2 (and I_2) and especially G_3 (and I_3) decrease more slowly than G_1 (and I_1). In a pure wodon case (final stage), $G_1(1) = G_2(1) = G_3(1) = 0.5$.

In this wodonization case, we assume that the eddy decays, not by decreasing its radius, but instead by deforming against the wall. This translates as $dR/dt = 0$ and $dH/dt = 0$. So, from (22) and (25) we get

$$\frac{dI_1}{dt} = -2R^2\sqrt{\delta(2-\delta)}\frac{d\delta}{dt}, \quad \frac{dI_2}{dt} = -\frac{4R^4}{3}\left[\delta(2-\delta)\right]^{3/2}\frac{d\delta}{dt}. \tag{27}$$

Since

$$V = V_b + I_1 H, \tag{28}$$

it follows from (22), (26) and (27) that

$$\frac{dV}{dt} = -\left[\frac{\alpha(2-\alpha)f_0^2R^2}{6g'}\delta(2-\delta) + 2H\right]R^2\sqrt{\delta(2-\delta)}\frac{d\delta}{dt}. \tag{29}$$

Substitution of (23), (24) (29) and (9) into (8) gives the final differential equation that models the eddy deformation against the wall,

$$\frac{\pi\beta R}{8}\left[\frac{\alpha(2-\alpha)f_0^2R^2}{24g'}G_3(\delta) + G_2(\delta)H\right]$$
$$-\left\{\frac{(2-\alpha)f_0^2R^2}{48g'}\left[3\pi G_2(\delta) + 4\alpha\delta(2-\delta)\sqrt{\delta(2-\delta)}\right] + H\sqrt{\delta(2-\delta)}\right\}\frac{d\delta}{dt} = 0, \tag{30}$$

whose solution is

$$t=\frac{4}{\pi\beta R}\int_0^{\delta}\frac{48g'H\sqrt{\delta(2-\delta)}+(2-\alpha)f_0^2R^2\left[3\pi G_2(\delta)+4\alpha\delta(2-\delta)\sqrt{\delta(2-\delta)}\right]}{24g'HG_2(\delta)+\alpha(2-\alpha)f_0^2R^2G_3(\delta)}d\delta. \qquad (31)$$

The integrand in (31) is always positive, even for cyclonic eddies ($\alpha<0$). In the last case, the denominator is positive because of the non-outcropping condition (16).

At $t=0$, it follows from (30) that the eddies' propagation speed is

$$C_{xi}=-R\frac{d\delta}{dt}=-\beta\left[\frac{\alpha R^2}{12}+\frac{2g'H}{(2-\alpha)f_0^2}\right],$$

which coincides with the eddy propagation speed in the open ocean [Zharkov and Nof, 2008b, Eq. (2)]. At the time the eddy is transformed into a wodon ($\delta=1$), we obtain

$$C_{xf}=C_{xi}\left[1+\frac{8\alpha}{3\pi}+\frac{32g'H}{\pi(2-\alpha)f_0^2R^2}\right]^{-1}. \qquad (32)$$

For the zero PV lenses ($\alpha=1,\ H=0$), we have $C_{xf}=C_{xi}/(1+8/3\pi)\approx 0.541C_{xi}$, which is larger than $C_{xi}/3$ in the tangent scenario (Nof, 1999).

The solid lines in Figure 6a show the evolution of δ for an anticyclonic and a cyclonic eddy both with $R=50$ km and $H=500$ m, and a lens of the same radius. For comparison, the dashed lines represent the propagation speeds of eddies in the open ocean (if there were no wall). Figure 6b shows the decrease of the eddy volume (as a fraction of the initial value). The value $H=500$ m satisfies the non-outcropping condition (16) for cyclonic eddies, where the minimal value of h is $h(0)=137$ m. As expected, the encounter is stronger for non-lenses than for lenses. Here, we define the lagging period as the difference between the time an eddy takes to transform into a wodon and the time it would take to propagate at a distance equal to its radius in the open ocean i.e., R/C_{xi}. In Figure 6a, this is the interval δ_l between the points where the solid and dashed lines of the same color reach the upper border. We can see that δ_l does not depend strongly on *H*. For lenses, the leakage (i.e., the volume decreasing rate, see Fig. 6b) is initially very small but later intensifies. If *H* is sufficiently large, for both an anticyclone and a cyclone, the leakage does not strongly depend on time. We note that Figure 6 is idealized because, as we will show, an eddy cannot turn completely into a wodon, and wodonization of lenses is unlikely.

c) Quantitative comparison of the theoretical formulas for encounter scenarios with numerics

To test our formulas for the eddy decaying velocity C ($= dR/dt$) in both scenarios, we compare the theoretical and numerical values of dR/dt for the conditions of Figure 3 (left panel for tangent scenario and right panel for wodonization) and for lenses with the same parameters, except $H = 0$ (tangent scenario). We average the parameters between the 150$^{\text{th}}$ and 200$^{\text{th}}$ days of simulation for lenses and the 20$^{\text{th}}$ and 40$^{\text{th}}$ days for non-lenses (which propagate much faster), when the eddy distortion is not yet strong enough to significantly complicate the measurement of *R* in the snapshots. The results are given in Table 1, where we list the characteristic parameters *R*, *H*, α, and δ (where the indices *i* and *a* indicate the initial and averaged values, respectively); estimated and numerical values of C (C_E and C_N, respectively); and the ratios C_N/C_E. We recall that the value of α (being one initially) is strongly altered by viscosity, so that its values (based on the eddy orbital velocity) at the moment of encounter are about 0.25 (in the tangent scenarios) and 0.36 (in the wodonization scenario). Also, the eddy radius increases during the alteration (before the contact with the wall), so that $R_a > R_i$. As a result, the ratio between numerical and theoretical values in the tangent scenario is 0.45 for lenses and 0.52 for non-lenses, respectively, and 0.81 in the wodonization scenario. It is not surprising that these values are less than one because, in the numerics, the propagation of eddies is usually slowed down by viscosity. As an example, the ratios between numerical and theoretical values of the eddy propagation speed *with no obstacles* are usually of the order 0.5 and even less (see, e.g. Zharkov and Nof, 2008a, Fig.9a).

d) Image effect

Shi and Nof (1994) argued that the eddy along-wall migration speed due to the image effect is of the same order as the orbital speed. In fact, this scale seems to be too large (one to a few meters per second). Here, on the basis of Shi and Nof's (1994) principle (using an heuristic approach), we try to obtain more realistic estimates of the image effect-induced migration speed.

A schematic plot showing the configuration of eddy–wall interaction is shown in Figure 7 (a modification of Fig. 1) in which the mirror-reflection of the arc ACB is shown as AC_1B. Also, we plot a vector indicating the direction of imaginary "flow into the wall," which is important since, theoretically, the image effect occurs mainly because there is no such flow. The direction of v_θ at point A (where the eddy touches the wall, Fig. 7) is represented by an inclined vector. According to the notations in subsection 4b, the speed of the imaginary flow into the wall is,

$$v_{I0} = v_\theta \sin\varphi = v_\theta \sqrt{\delta(2-\delta)}, \tag{33}$$

where, as before, $\delta = b/R$. Since we assume that the wall reflects the fluid particles, (33) defines the characteristic speed of particles inside the region bound by the wall and the arc AC_1B, i.e., the particles in the volume V_{AC_1B}. However, we should consider the movement of the entire volume of the "truncated" eddy (i.e., the "squeezed" circle with the segment ACB cut out). Therefore, the image effect-induced propagation speed is

$$v_I = v_{I0} \frac{V_{AC_1B}}{V_{AEB}}. \tag{34}$$

According to (22) and (23), we have

$$V_{AEB} = I_1 H + \frac{\alpha(2-\alpha) f_0^2}{8g'} I_2. \tag{35}$$

Also, assuming that $V_{AC_1B} = V - V_{AEB}$, we obtain from (12), (34), and (35) an estimate of the truncated eddy propagation speed

$$v_I = v_\theta \sqrt{\delta(2-\delta)} \frac{16g'H\left[1-G_1(\delta)\right] + \alpha(2-\alpha) f_0^2 R^2 \left[1-G_2(\delta)\right]}{16g'HG_1(\delta) + \alpha(2-\alpha) f_0^2 R^2 G_2(\delta)}, \tag{36}$$

where G_1 and G_2 are expressed by (22) and (25).

To test (36), we compare the theoretical results with numerics under the conditions of Figure 3 (right panel), using the same parameters, except $H = 300$ m. We note that, at the beginning of numerical run, the eddy accelerates along the meridional wall. So, to exclude that period, we average all results between the 50th and 100th days of simulation. The results are given in Table 2. Here we list the same parameters as in Table 1 along with v_θ (initialized and averaged), values of v_I estimated theoretically by (36) and its numerical values (v_{IE} and v_{IN}, respectively) and the ratios v_{IN} / v_{IE}. We note here that, (i), in Table 1 (focused on the eddy center zonal propagation speed), the data are averaged between the 20th and 40th days (which is the eddy meridional acceleration period), so α_a and δ for the same experiment with $R_i = 100$ km and $H = 500$ m are different in Tables 1 and 2; and (ii), unlike C_E, v_{IE} is expressed through the orbital velocity that is already altered by viscosity during the experiment. Therefore, the effect of viscosity on the ratio v_{IN} / v_{IE} is weak, so values more than one are suitable. On the basis of the v_{IN} / v_{IE} values, we suggest that (36) gives a satisfactory estimate of the image speed.

e) Notes about realization of scenarios and image effect in the theoretical model and the numerics.

We have already mentioned that the tangent scenario with no image effect characterizes the encounter process for lenses in any condition, and for non-lenses when the boundary condition at the wall is no-slip. In the case of FSBC, a non-lens eddy is expected to squeeze according to the wodonization scenario and, at the same time, propagate along the wall because of the image effect.

Note that, in (36), we do not take the leakage into account. If we do, the expression (36) for v_I should be multiplied by $(1 - L)$ with L the leakage coefficient, which is the ratio of the leakage volume and V_{ACB}. From (8), we obtain the leakage volume transport dV / dt but it is difficult to determine over which period of time it should be integrated. However, we showed in subsection 2a that $l \sim \varepsilon R_d \sim 0.35 \varepsilon R$, so the assumption that l is small compared to b should be valid as well (excluding a very short period of time at the beginning of the encounter when the eddy propagation along the wall is still accelerating). Indeed, in Table 2, the values of δ are much larger than 0.35ε, which is about $3.1 \cdot 10^{-3}$ for the considered value of R and latitude of, say, Brazil-Malvinas convergence.) Since l and b characterize the zonal scales of leakage and ACB, respectively, and the meridional scales are comparable, we can assume that the leakage volume is much smaller than V_{ACB}. Hence $L \ll 1$, and the inherent error is small.

Also, there is an alternative choice of denominator in (34). We can use V (the entire eddy volume) instead of V_{AEB} because there are both non-reflected and reflected particles inside the segment AC_1B (Fig. 7). However, the difference is $O\left(\delta^{5/2}\right)$ for lenses and $O\left(\delta^{3/2}\right)$ for cylindrical eddies. For real eddies, it is $O\left(\delta^{2}\right)$, which is about 15-20% in our cases and also comparable with errors inherent in all other assumptions. So, (36) is approximately valid.

It can be seen from our numerics that the wodonization is not complete but stops at some intermediate stage and, beyond that point, the eddy volume decreases according to the tangent scenario though the area of eddy–wall contact is large. The value of δ, at this stage, remains almost constant, so the image propagation speed is approximately constant as well. An estimation of that speed can be derived by analogy with the case of "viscous image effect" on an f-plane, as will be considered in the next section. Such an assumption is based on the idea that, if δ is constant, the β–effect is not important.

Finally, when the eddy reaches the northwestern corner of the simulation area (for the Northern Hemisphere), it gets locked there and gradually dissipates.

5. "Viscous image effect" on an *f*-plane

In the preceding section, we considered the eddy–wall encounter on a β-plane resulting from the usual westward propagation. Theoretically, baroclinic rings cannot propagate on an *f*-plane, and we should not expect any eddy–wall interaction without β. Nevertheless, in numerical experiments, some anomalous effects appear that cannot be explained by an idealized non-viscous model without taking into account the boundary conditions.

Here we analyze one of these anomalous effects. Figures 8 and 9 show the simulations with eddies whose parameters are $R = 100$ km, $\alpha = 1$ (initially), and $H = 300$ m (Fig. 8) and 500 m (Fig. 9). Analogous with Figure 3, left panels show simulations with NSBC, and right panels with FSBC. For all the simulations, the viscosity coefficient ν is 50 $\mathrm{m^2\,s^{-1}}$ (which gives a diffusion speed of 0.01 $\mathrm{m\,s^{-1}}$). The initial condition is an anticyclone tangent to the wall on an *f*-plane, approximately 400 km off the lower border of the calculation area.

As seen in the figures, in the case of FSBC, an anticyclonic eddy initially tangent to the wall starts to propagate northward along it (in the Northern Hemisphere) and then goes clockwise around the square/rectangular domain area until it completely dissipates. Under NSBC, such an eddy does not propagate. On the whole, the eddy behaves similarly to the simulations on a β-plane. The main qualitative difference is that, with FSBC, the eddy is not locked at the northwestern corner but continues to move along the walls (see the lower right panel in Fig. 9).

As expected, the propagation speed strongly depends on the eddy basement depth H (i.e., depth of the upper layer at the rim of the eddy, see Fig. 2). As a side effect, if the depth of the eddy is relatively large, some weaker vortices (cyclonic in this particular case) appear and translate in the opposite direction (Fig. 9, right panels) in agreement with Shi and Nof (1993). In the case of FSBC, a single companion eddy goes around the perimeter of the simulation area counterclockwise (and even bypasses the main eddy when re-encountering it – not shown). In the case of NSBC, two very weak cyclones rotate around the main eddy but dissipate quickly.

From our analysis, it seems that even on an f-plane, the image effect also occurs in the case of FSBC. We suggest that this is an artifact of numerical simulations due to the viscosity. At the beginning of the experiment, the vorticity of eddy decreases, while its radius grows slightly. Under the NSBC, the eddy continues to be tangent to the wall, similar to an "elastic ball." Under the FSBC, the distance between the eddy center and the wall remains approximately constant, so the eddy actually squeezes onto the wall, leading to the image effect. In the displayed simulations, the viscosity coefficient is small, so, initially, the eddy accelerates in the meridional direction very slowly, and its shape is not quite circular. Both the squeeze and the more stable propagation start after a certain period of time.

To better understand this image effect, we also simulate encounters for eddies with smoothed orbital velocity profiles, as

$$v_\theta = -\frac{\alpha f_0}{2}\left(r - \frac{r^{n+1}}{R^n}\right),\ n = 1,2,3,... \tag{37}$$

From (10) and (37) we obtain

$$h = \frac{\alpha f_0^2 R^2}{4g'} \left\{ \left(1 - \frac{\alpha}{2}\right)\left[1 - \left(\frac{r}{R}\right)^2\right] - \frac{2(1-\alpha)}{n+2}\left[1 - \left(\frac{r}{R}\right)^{n+2}\right] - \frac{\alpha}{2(n+1)}\left[1 - \left(\frac{r}{R}\right)^{2(n+1)}\right] \right\} \tag{38}$$
$$+ H.$$

In the case of $n = 1$, the structure of v_θ is parabolic.

Also, we simulate the Gaussian eddies with

$$h = H + h_0 \exp\left[-\left(r / r_0\right)^2\right], r \le R;\; h = H,\; r > R, \tag{39}$$

$$v_\theta = -\frac{r f_0}{2}\left[\sqrt{1 + \frac{8 g' h_0}{\left(f_0 r_0\right)^2} \exp\left[-\left(r / r_0\right)^2\right]} - 1\right],\; r \le R;\;\; v_\theta = 0,\; r > R. \tag{40}$$

Figure 10 shows snapshots for the Gaussian eddies in the case of FSBC; the parameter values are given in Table 3, the second row from the bottom. Unlike the preceding figures, the left panel shows the evolution of vector-velocities of the eddy particles. The basin size is 2000×2000 km, and, at the initial moment of time, the eddy is centered at $x = 250$ km and $y = 1000$ km. It is seen that, qualitatively, there are no significant differences with the cases described above, although the leakage of the eddy looks somewhat stronger. Also, it can be inferred from the left panel that, as a result of the "image effect," the particles at the wall strongly accelerate at the moment of their detachment (at the upper point of the eddy–wall contact area). As before, in the NSBC case, the image effect is absent. For smoothed profiles (not shown), the snapshots are qualitatively similar. Therefore, we can consider only quantitative differences in the behavior of eddies with linear, smoothed, and Gaussian structures.

As an argument in favor of our conclusion that the considered image effect is caused by viscosity, we note that the viscosity is the main factor defining the propagation speed. Actually, it acts in two ways. On one hand, the viscosity causes the growth of the eddy radius, increasing δ and, therefore, accelerating the eddy. On the other hand, it slows the orbital velocity and, therefore, the propagation speed as well. Consequently, the eddy accelerates initially, propagates with almost constant speed for a while, and then slows. The period of this cycle significantly shortens for large viscosity, especially for eddies with linear profiles of v_θ.

We assume that when the propagation speed is nearly constant, it can be estimated using (36), by analogy with the image effect in the wodonization case. It is obvious that, if we use (37) and (38) or (39) and (40) instead of (7) and (11), all formulas in Section 4 are not valid, excepting (10). Nevertheless, we test whether (36) can give a fair estimate of the propagation speed in these cases as well by taking v_θ as the maximal radial speed. The results are given in Table 3, where the parameter notations are the same as in Table 2. In numerics, we calculate the characteristic values of v_I by averaging data from the 100th to the 200th day of simulation, except for the large viscosity cases, for which we averaged data from the 50th to the 150th day, and small viscosity and linear v_θ profile, for which we averaged data from the 150th to the 250th day. Unfortunately, v_{IN} / v_{IE} is not accurate because (36) is strongly nonlinear, so that, on average, the nearly 15% uncertainty in experimental estimation of δ (which comes mainly from deformations of the eddy in numerical simulations) leads to about 40% uncertainty in the calculation of v_{IE}.

It is seen from Table 3 that, despite the aforementioned uncertainty, (36) is suitable for estimating the speed except for cyclonic eddies. (In this case, the theoretical results are almost of the order of the orbital speed but the experimental values are much larger than for anticyclonic eddies as well.) For large values of viscosity, as expected, the smoothed eddies propagate slower than those with a linear profile of v_θ. However, for small viscosity, eddies with smoothed profiles of v_θ propagate faster than ones with a linear profile. This is because, for *smoothed profiles* (rows 10–15 in the main body of Table 3), the characteristic δ weakly depends on the viscosity (probably because of gentle "adaptation" of the velocity distribution to the encountering process), so, with increasing ν, the decrease of maximal orbital velocity becomes an overwhelming factor that slows the propagation. In contrast, in the case of *linear* velocity profile (and zero PV initially, see rows 1–6 in the main body of Table 3), the characteristic value of δ significantly grows with increasing viscosity, and so does the propagation speed. The effect of decreasing initial value of α is analogous to smoothing the profile (though δ does grow with increasing viscosity but not as strongly as in the case of zero PV initially). Also, as should be the case, the propagation speed increases with growing *H*.

Finally, we note that in Section 4 (simulations on a β-plane), we considered the eddy initially centered at a distance equal to its diameter from the wall. In that case, the viscous adjustment of the eddy was almost completed when it touched the wall. So, in the case of FSBC, the image effect was entirely caused by the β-effect. However, in some runs with an eddy initially touching the wall on a β-plane (not shown in the figures), the viscous extension was the strongest factor defining the eddy along-wall propagation speed, overwhelming the β-effect. We do not suggest that this is common because it depends on the eddy initial parameters.

6. Conclusions and discussion

Eddies' encounters with a meridional wall and their subsequent along-wall propagation are investigated using one-and-half layer analytical and numerical models. Such an investigation can be applied to dynamics of eddies in many regions of the world's oceans (Nof, 1999) [though, in some cases, the western boundary currents complicate this process (see, e.g. Byrne et al., 1995, for Agulhas eddies)].

In the Northern Hemisphere, the results can be summarized as follows:

1. The behavior of a non-lens eddy encountering a wall strongly depends on the boundary condition. In the case of a no-slip boundary condition (tangent scenario), the encounter is quite similar to the case of lenses described by Nof (1999). The eddy barely propagates along the wall and gradually leaks. The rate of the decrease in the radius is $1/\left\{1+\alpha\beta R_0 t/\left[12\left(2\alpha+1\right)\right]\right\}$ for lenses and $1/\left(1+\beta R_0 t/8\right)$ for deep upper-layer eddies (the latter approximation is probably valid even when the depth of the environmental upper layer H is of the same order as the height of the eddy bell).
2. In the case of a free-slip boundary condition (wodonization scenario), the eddy squeezes against the wall, and because of dissipation, the center approaches the wall significantly faster than it does in the tangent case. The approaching speed increases with growing H. Also, the image effect is significant. For both dissipation rate and along-wall speed, the formulas are obtained in terms of orbital velocity and coefficient of squeezing (defined in Section 2).
3. In the wodonization case, the eddy does not transform completely into a wodon. Rather, the coefficient of squeezing reaches approximately 0.6 and then remains almost constant during the dissipation period.

4. In *f*-plane numerical simulations, a non-lens baroclinic eddy initially tangent to a free-slip wall is subjected to a viscous image effect, and its along-wall propagation speed can be roughly estimated with the same formula used in the *β*-plane encounters.
5. Our formulas are in adequate agreement with numerical experiments except for the very strong viscous image effect over cyclonic eddies.

Though the numerical simulations of a single eddy do not require strong viscosity coefficients for stability, it would be interesting, in the future, to consider less viscous numerical models, like QG-models. Also, in considering the eddy propagation along the wall, we do not take into account the effect of possible self-propagation of baroclinic eddies (Radko and Stern, 1999, 2000). In our *f*-plane simulations, if the distance between the initialized eddy and the wall were equal to the eddy diameter, this eddy could not move. Possibly the effect of finite depth can significantly affect the behavior of such an eddy.

Finally, we did not consider how the wall boundary conditions (which are artificial in numerics) are related to the real character of the continental coast and the nearshore oceanic area. In real conditions, we know intuitively that the tangent scenario of encountering is more likely to occur than the wodonization. However, the eddy is more likely to propagate along the wall than to stay at the same location (though, according to observations, anticyclionic eddies can go both poleward and equatorward after encountering the wall – see Shi and Nof, 1994). Probably the free-slip boundary condition is a more natural condition because, in fact, the wall is not vertical and the entire eddy basement cannot attach to it all at once. Although we do not take into account the bottom topography when considering the eddy propagation, the wall can be considered a line behind which the real depth is less than some chosen value. This value can be, for example, of the order of double or triple the Ekman layer depth, the characteristic depth of the upper layer, the depth of a narrow continental bank, etc. In any case, the real bathymetry can stop the movement of the eddy's deep part, while its shallow part can both go across the line of "wall" and slip along it. Since the behavior of the encountering eddy strongly depends on the type of boundary condition, we expect its strong dependence on the steepness of the continental slope and bottom topography. Several papers consider the interaction of eddies with continental slope topography (see, e.g., Frolov et al., 2004; Sutyrin et al., 2009), though the investigations focus mainly on quasigeostrophic eddies, which are relatively weak. Future studies might examine the effect of topography for the wide diversity of eddies.

APPENDIX A. Contour integration and neglect of small terms in governing equation (6).

As we assume that the disturbances outside the eddy and leakage are small, we rewrite the first term as

$$\oint_{\partial S}\left(-hv^2+f\psi-\frac{g'}{2}h^2\right)_l dx+\oint_{\partial S}\left(-hv^2+f\psi-\frac{g'}{2}h^2\right)_e dx, \tag{A1}$$

where the indices l and e mean the contributions from leakage and the eddy. In the first term, the contour ∂S can be reduced to PP_1 (i.e., the crosscut of the leakage, see Fig. 1.) As we assume that, in the first approximation, the leakage is geostrophic, and f does not strongly change inside the considered area, we can neglect $\left(f\psi - g'h^2/2\right)$ in this term, so that, in the zero-order in expansion by ε, we have

$$\oint_{\partial S}\left(-hv^2 + f\psi - \frac{g'}{2}h^2\right)_l dx = -\int_{P}^{P_1} hv^2\, dl. \qquad \text{(A2)}$$

In the second integral in (A1) that expressed the "non-leaking eddy" contribution, we can assume that, outside the eddy, H is constant, and u and v are at least of the next order of smallness compared to the liquid velocities inside the eddy and the leakage. Here, we again introduce the expansions analogous to (3.1) in Nof (1999) and use the "small distortion approximation." Now, we estimate $\oint_{\partial S}\left(-hv^2 + f\psi - \frac{g'}{2}h^2\right)_e dx$, following Nof's (1983) approach. We assume that our solution is slowly varying in time, so that the Bernoulli function in a moving coordinate system

$$G(\psi) = \frac{1}{2}\left(u^2+v^2\right) + g'\left(h-H\right) + \left(f_0 + \frac{\beta y}{2}\right)Cy$$

is constant along an arbitrary streamline. In application to the rim of the eddy, we have

$$\frac{1}{2}\left(u^2+v^2\right) + g'(h-H) + \left(f_0 + \frac{\beta y}{2}\right)Cy = \frac{C^2}{2} + \left(f_0 + \frac{\beta y_0}{2}\right)Cy_0,$$

where y_0 the latitude of $\psi = 0$ far away from the eddy; u, v, and h are calculated at the eddy boundary. Therefore,

$$h = H + \frac{1}{2g'}\left(C^2 - u^2 - v^2\right) - \frac{1}{g'}\left(f_0 + \frac{\beta y}{2}\right)Cy + \frac{1}{g'}\left(f_0 + \frac{\beta y_0}{2}\right)Cy_0 \qquad \text{(A3)}$$

and

$$\frac{g'}{2}h^2 = \frac{1}{2g'}\left\{\frac{\left(C^2-u^2-v^2\right)^2}{4}+\left[g'H-\left(f_0+\frac{\beta y}{2}\right)Cy+\left(f_0+\frac{\beta y_0}{2}\right)Cy_0\right]\left(C^2-u^2-v^2\right)\right.$$

$$+\left(g'H\right)^2+\left(f_0+\frac{\beta y}{2}\right)^2C^2y^2+\left(f_0+\frac{\beta y_0}{2}\right)^2C^2y_0^2-2g'H\left(f_0+\frac{\beta y}{2}\right)Cy$$

$$\left.+2g'H\left(f_0+\frac{\beta y_0}{2}\right)Cy_0-2\left(f_0+\frac{\beta y}{2}\right)\left(f_0+\frac{\beta y_0}{2}\right)C^2yy_0\right\}.$$

As a result,

$$\oint_{\partial S}\left(-hv^2+f\psi-\frac{g'}{2}h^2\right)_e dx$$

$$=\frac{1}{2g'}\oint_{\partial S}\left\{-\frac{\left(C^2-u^2-v^2\right)^2}{4}-\left[g'H-\left(f_0+\frac{\beta y}{2}\right)Cy+\left(f_0+\frac{\beta y_0}{2}\right)Cy_0\right]\left(C^2-u^2+v^2\right)\right.$$

$$-\left(g'H\right)^2-\left(f_0+\frac{\beta y}{2}\right)^2C^2y^2-\left(f_0+\frac{\beta y_0}{2}\right)^2C^2y_0^2+2g'H\left(f_0+\frac{\beta y}{2}\right)Cy \tag{A4}$$

$$-2g'H\left(f_0+\frac{\beta y_0}{2}\right)Cy_0+2\left(f_0+\frac{\beta y}{2}\right)\left(f_0+\frac{\beta y_0}{2}\right)C^2yy_0$$

$$\left.-\left(C^2-u^2-v^2\right)v^2+2g'\left(f_0+\beta y\right)\psi\right\}dx.$$

Some terms are constant (we recall that H is also constant), so their contributions to the integral vanish and (A4) becomes

$$\oint_{\partial S}\left(-hv^2+f\psi-\frac{g'}{2}h^2\right)_e dx$$

$$=\frac{1}{2g'}\oint_{\partial S}\left\{-\frac{\left(C^2-u^2-v^2\right)^2}{4}-\left[g'H-\left(f_0+\frac{\beta y}{2}\right)Cy+\left(f_0+\frac{\beta y_0}{2}\right)Cy_0\right]\left(C^2-u^2+v^2\right)\right. \tag{A5}$$

$$-\left(f_0+\frac{\beta y}{2}\right)^2C^2y^2+2g'H\left(f_0+\frac{\beta y}{2}\right)Cy+2\left(f_0+\frac{\beta y}{2}\right)\left(f_0+\frac{\beta y_0}{2}\right)C^2yy_0$$

$$\left.-\left(C^2-u^2-v^2\right)v^2+2g'\left(f_0+\beta y\right)\psi\right\}dx.$$

Although we consider the "contribution from the eddy" in (A1), the contour ∂S encloses the eddy from outside (which can be considered a streamline bordering the eddy), so the summation of the terms with v in (A5) is valid. If we assume that, along ∂S, both u and v are of the order of C, the horizontal scale is R_d, and the time scale is f_0^{-1}, then $\{x, y, y_0\} \sim R_d$ and $g'H \sim (R_d f_0)^2$ in the common case. Furthermore, $\{C, u, v\} \sim \beta R_d^2 \sim \varepsilon R_d f_0$, and $\beta y \sim \varepsilon f_0$. Also, because ψ is constant along a streamline, the only contribution to the last term in the braces is across the "imaginary" leakage, i.e., the segment PP_1. In subsection 2a we showed that, for non-lenses, l (which is the length of PP_1) is of the order εR_d. [For lenses, $l \sim \varepsilon^{1/2} R_d$ but the results are basically the same (Nof, 1999).] Hence, $2g' \oint\limits_{\partial S} (f_0 + \beta y)\psi\, dx$ is of the order $\varepsilon g' f_0 h u x^2 \sim \varepsilon^2 R_d (R_d f_0)^4 (h / H)$, where h is again expressed by (A3).

Therefore, there are no terms of the order ε^0 in the braces in the right-hand side of (A5), and the only term of the order ε^1 is $2g'Hf_0Cy$. So, with error $O(\varepsilon^2)$, we can write

$$\oint\limits_{\partial S} \left(-hv^2 + f\psi - \frac{g'}{2} h^2 \right)_e dx = Cf_0 H \oint\limits_{\partial S} y\, dx = -Cf_0 H S_e. \tag{A6}$$

Taking into account (A1), (A2), and (A6) in (6), we obtain (7), where the integration area in the term with β is S_e because this term describes the β-force due to the eddy rotation, and the contribution from the area outside the eddy is negligible.

APPENDIX B. List of abbreviations and symbols

b – width of the squeezed segment of eddy

$C(t)$ – zonal westward propagation speed of the eddy

C_{xi}, C_{xf} – value of $C(t)$ at the beginning of squeezing and at the moment when the eddy (theoretically) becomes a wodon

f – Corilois parameter

f_0 – local absolute value of f

FSBC – free-slip boundary condition

g' – reduced gravity

$G_i(\delta)$ ($i = 1, 2, 3$) – dimensionless functions defined by (22), (25), (26)

h – depth of upper (disturbed) layer

h^* – depth of leakage

H – value of h outside the eddy (“basic” depth)

$\tilde{h}(= h - H)$ – disturbed part of h (in the eddy area – depth of the eddy bell)

I_1, I_2, I_3 – integrals defined by (22), (25), (26)

l – width of leakage

n – parameter of smoothness of the eddy orbital velocity profile in (37)

NSBC – no-slip boundary condition

PV – potential vorticity

R – eddy radius

R_0 – initial value of R

R_d – eddy Rossby radius

Ro – Rossby number

S – overall integration area

S_e – eddy integration area

t – time

u, v – horizontal velocity coordinates

V – eddy volume

V_b – eddy bell volume

v_θ – orbital velocity of the eddy

v_{I0} – projection of v_θ on the x-axis

v_I – eddy propagation velocity owing to the image effect

v_{IN} – value of v_I in the numerics

v_{IE} – theoretical value of v_I calculated by (36)

$v_{\theta i}, v_{\theta a}$ – initial and time-averaged values of the eddy maximal orbital speed in numerics

x, y – horizontal coordinates

α – eddy vorticity parameter

β – meridional gradient of the Coriolis parameter

δ – coefficient of squeezing (b / R)

ε – small parameter equal to $\beta R_d / f$

ν – viscosity coefficient (in numerics)

$\Delta\rho$ – difference between densities of the lower and upper layers of water

ρ – density of the lower oceanic layer

φ – angle of squeezing visibility from the center of the eddy (Fig. 1)

ψ – streamfunction

Acknowledgments. The study was supported by NASA Doctoral Fellowship Grant NNG05GP65H; LANL/IGPP Grant (1815); NSF (OCE-0752225, OCE-9911342, OCE-0545204, OCE-0241036), BSF (2006296), and NASA (NNX07AL97G). (Eric and Alex, please list your grants!) Wilton Arruda is supported by Conselho Nacional de Desenvolvemento Cientifico e Tecnologico (CNPq), of the Ministry of Science and Technology of Brazil, under grant 201627/2010-8. We are grateful to Steve Van Gorder for helping in the numerical simulations. We also thank Donna Samaan for helping in preparation of the manuscript and Kathy Fearon for assistance in improving the style.

References

Azevedo, J. L. L., D. Nof, and M. M. Mata, 2012: Encounters of eddies trains with a continental boundary. *J. Phys. Oceanogr.,* **42**, 1548-1565.

Bleck, R., and D. Boudra, 1986: Wind-driven spin-up in eddy-resolving ocean models formulated in isopycnic and isobaric coordinates, *J. Geophys. Res.*, **91**, 7611-7621.

Burne, D. A., A. L. Gordon, and W. F. Haxby, 1995. Agulhas eddies: A synoptic view using Geosat ERM data. *J. Phys. Oceanogr.,* **25**, 902-917.

Frolov, C. A., G. G. Sutyrin, G. D. Rowe, and L. M. Rothstein, 2004. Loop Current eddy interaction with the western boundary in the Gulf of Mexico. *J. Phys. Oceanogr.*, **34**, 2223-2237.

Kundu, P. K., and I. M. Cohen, 2008: *Fluid Mechanics*, Academic Press, Elsevier, 4th Ed., 878 p.

Lamb, H., 1932: Hydrodynamics, Cambridge University Press, Cambridge, 738 pp.

Masuda, A., 1988: A skewed eddy of Batchelor-modon type. *J. Ocean. Soc. Japan*, **43**, 383-394.

Minato, S., 1982: Geostrophic adjustment near the coast. *J. Ocean. Soc. Japan*, **38**, 225-235.

Minato, S., 1983: Geostrophic response near the coast. *J. Ocean. Soc. Japan*, **39**, 141-149.

Nof, D., 1983: On the migration of isolated eddies with application to Gulf Stream rings. *J. Mar. Res.*, **41**, 399-425.

Nof, D., 1988a: Draining vortices. Geophys. Astrophys. Fluid. Dyn., 42, 187-208.

Nof, D., 1988b: Eddy-wall interactions. *J. Mar. Res.*, **46**, 527-555.

Nof, D., 1999: Strange encounters of eddies with walls. *J. Mar. Res.*, **57**, 739-761.

Pierrehumbert, R., 1980: A family of steady, translating vortex pairs with distributed vorticity. *J. Fluid Mech.*, **99**, 129-144.

Radko, T., and M.E. Stern, 1999: On the propagation of oceanic mesoscale vortices. *J. Fluid Mech.*, **380**, 39-57.

Radko, T., and M.E. Stern, 2000: Self-propagating eddies on the stratified *f* plane. *J. Phys. Oceanogr.*, **30**, 3134-3144.

Saffman, P., 1979: The approach of a vortex pair to a plane surface in inviscid fluid. *J. Fluid Mech.*, **92**, 497-503.

Shi, C., and D. Nof, 1993: The splitting of eddies along boundaries. *J. Mar. Res.*, **51**, 771-795.

Shi, C., and D. Nof, 1994: The destruction of lenses and generation of wodons. *J. Phys. Oceanogr.*, **24**, 1120-1136.

Sutyrin, G., A. Stegner, I. Taupier-Letage, and S. Teinturier, 2009. Amplification of a surface-intensified eddy drift along a steep shelf in the Eastern Mediterranean Sea. *J. Phys. Oceanogr*., **39**, 1729-1741.

Umatani, S., and T. Yamagata, 1987: Evolution of an isolated eddy near a coast and its relevance to the “Kyucho”. *J. Ocean. Soc. Japan*, **43**, 197-203.

Wu, H., E. Overman, and N. Zabusky, 1984: Steady-state solutions of the Euler equations in two dimensions rotating and translating V-states with limiting cases. I: Numerical algorithms and results. *J. Comput. Phys.*, **53**, 42-71.

Yasuda, I., K. Okuda, and K. Mizuno, 1986: Numerical study of the vortices near boundaries-considerations on warm core rings in the vicinity of east coast of Japan. Bulletin of Tohoku Regional Fisheries Research Laborartory, **48**, 67-86.

Zavala Sansón, L., F. Graef, and E.G. Pavia, 1998: Collision of anticyclonic, lens-like eddies with a meridional western boundary. *J. Geophys. Res.*, **103**, 24,881-24,890.

Zharkov, V., and D. Nof, 2008a: Retroflection from slanted coastlines-circumventing the “vorticity paradox”. *Ocean Sci*., 4, 293-306.

Zharkov, V., and D. Nof, 2008b: Agulhas ring injection into the South Atlantic during glacials and interglacials. *Ocean Sci*., 4, 223-237.

Table 1. Parameters and results of theoretical and numerical estimation of the eddy center migration speed in the eddy–wall encounters on a β-plane. Here and in Tables 2 and 3, indices *i* and *a* mean initial and averaged values, and *E* and *N* mean estimated (using a theoretical model) and numerical values.

Scenario	R_i, km	R_a, km	H, m	ν, m^2 s^{-1}	α_i	α_a	δ	C_N, km day^{-1}	C_E, km day^{-1}	C_N / C_E
tangent	100	110	0	350	1	0.25	0	0.15	0.33	0.45
	100	110	500	350	1	0.25	0	0.70	1.36	0.52
wodonization	100	130	500	350	1	0.36	0.21	2.75	3.41	0.81

Table 2. Parameters and results of theoretical and numerical estimations of image effect in the eddy–wall encounters on a β-plane.

R_i, km	H, m	ν, m^2 s^{-1}	α_i	α_a	$v_{\theta i}$, cm s^{-1}	$v_{\theta a}$, cm s^{-1}	δ	v_{IN}, km day^{-1}	v_{IE}, km day^{-1}	$\frac{v_{IN}}{v_{IE}}$
100	300	350	1	0.23	429	97	0.39	9.89	7.97	1.24
100	500	350	1	0.17	429	73	0.45	14.02	12.07	1.16

Table 3. Parameters and results of theoretical and numerical estimations of viscous image effect.

Vortex types	Orbital velocity structure	R_i, km	H, m	n	ν, $m^2\ s^{-1}$	α_i	α_a	$v_{\theta i}$, cm s^{-1}	$v_{\theta a}$, cm s^{-1}	δ	v_{IN}, km day^{-1}	v_{IE}, km day^{-1}	$\frac{v_{IN}}{v_{IE}}$
anti-cyclonic	linear	100	300	-	50	1	0.334	429	143.2	0.11	1.09	0.80	1.36
		100	300	-	100	1	0.252	429	108.2	0.24	3.45	3.17	1.09
		100	300	-	150	1	0.190	429	81.48	0.31	3.23	4.32	0.75
		100	300	-	250	1	0.135	429	57.80	0.32	2.55	3.39	0.75
		100	300	-	500	1	0.114	429	49.0	0.38	3.18	4.01	0.79
		100	500	-	50	1	0.458	429	196.5	0.26	5.64	7.84	0.72
		100	300	-	50	0.2	0.084	85.8	36.06	0.24	3.45	3.17	1.09
		100	300	-	100	0.2	0.067	85.8	28.70	0.36	1.64	2.39	0.69
		100	300	-	500	0.2	0.028	85.8	11.96	0.47	1.64	1.83	0.90
	smoothed	100	300	1	50	1	0.513	109.7	56.3	0.30	2.09	2.58	0.81
		100	300	4	50	1	0.472	235.3	111.1	0.33	4.64	6.01	0.77
		100	300	1	100	1	0.339	109.7	37.17	0.29	1.82	1.63	1.12
		100	300	4	100	1	0.317	235.3	74.72	0.31	2.82	3.73	0.76
		100	300	1	500	1	0.113	109.7	12.43	0.33	0.82	0.87	0.94
		100	300	4	500	1	0.114	235.3	26.72	0.27	1.06	1.16	0.91
	Gaussian	200	1000	-	500	-	0.40	141	56	0.42	2.5	4.47	0.56
cyclonic	linear	100	500	-	50	-1	-0.89	-209	-184.4	0.50	20.0	113.4	0.18

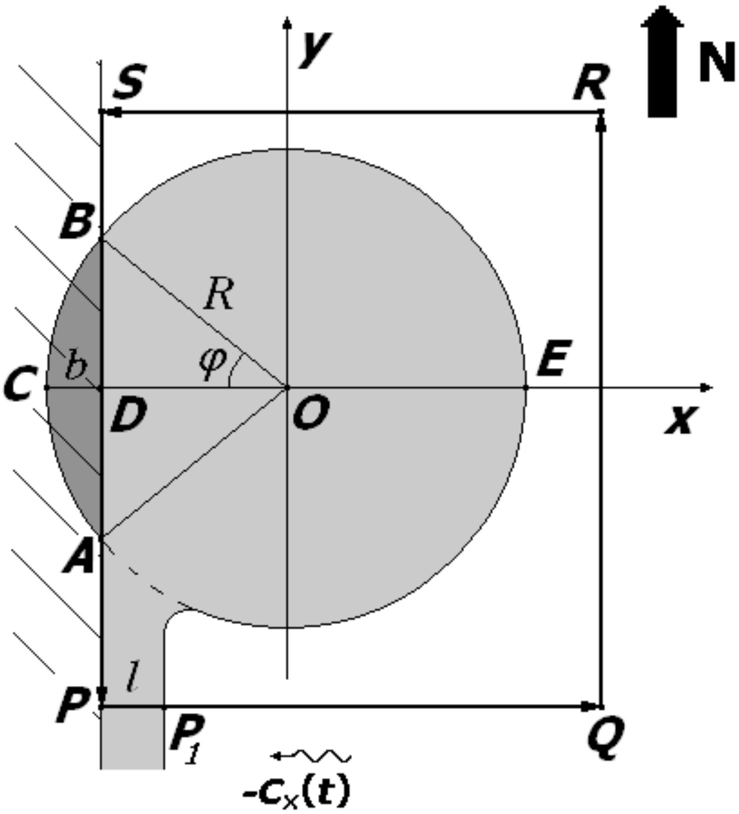

Figure 1. Schematic diagram of the study model. The eddy propagating westward encounters the meridional wall. Subsequently, the leaking along the wall occurs and the eddy squeezes gradually. The "wiggly" arrow shows the direction of the squeezing eddy propagation. The value of propagation velocity $C_x(t)$ is strongly reduced compared to the eddy propagation speed in the open ocean. Segment *ABC* is the squeezed area; *b* is its "deepening"; *PQRS* is the integration contour. PP_1 is the cross section of the leakage whose width is *l*.

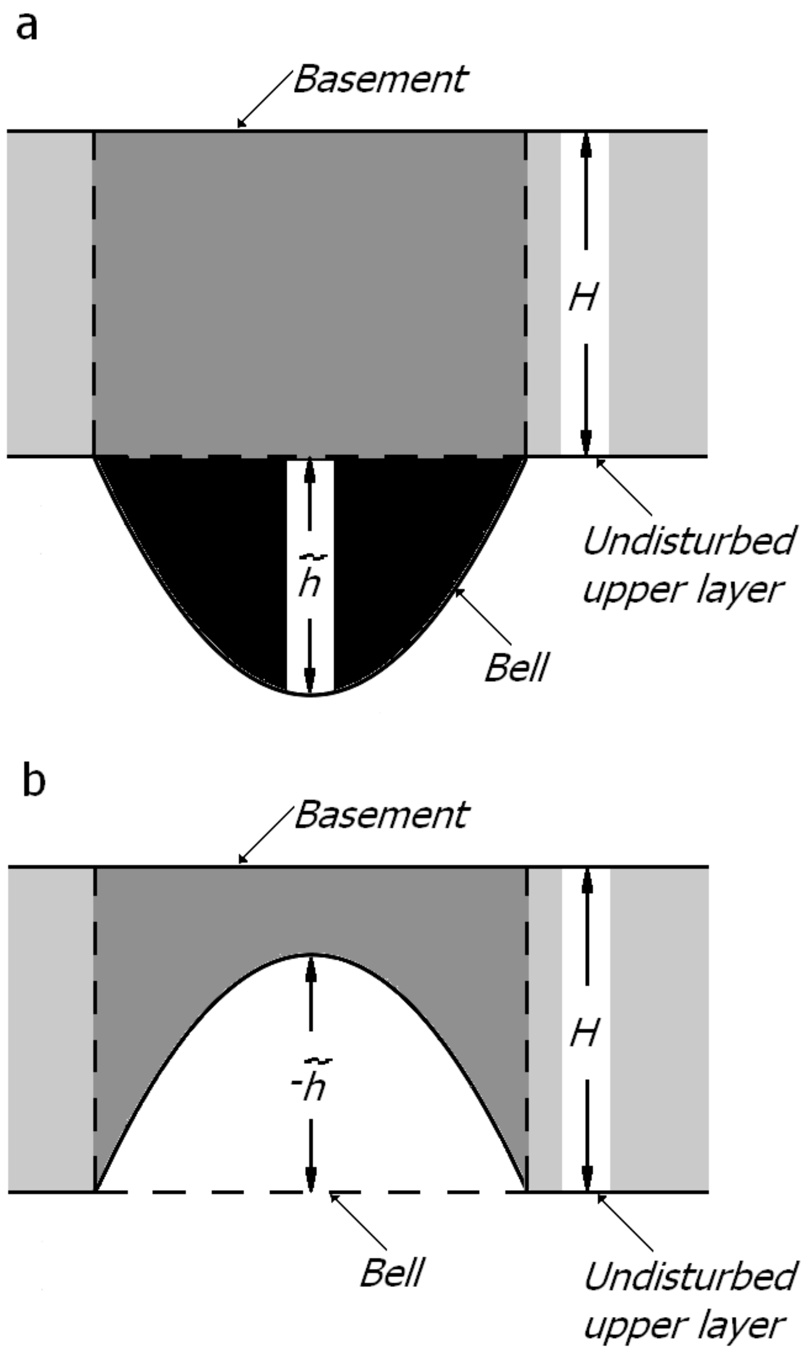

Figure 2. Structure and introduced notations for (a) anticyclonic and (b) cyclonic eddies.

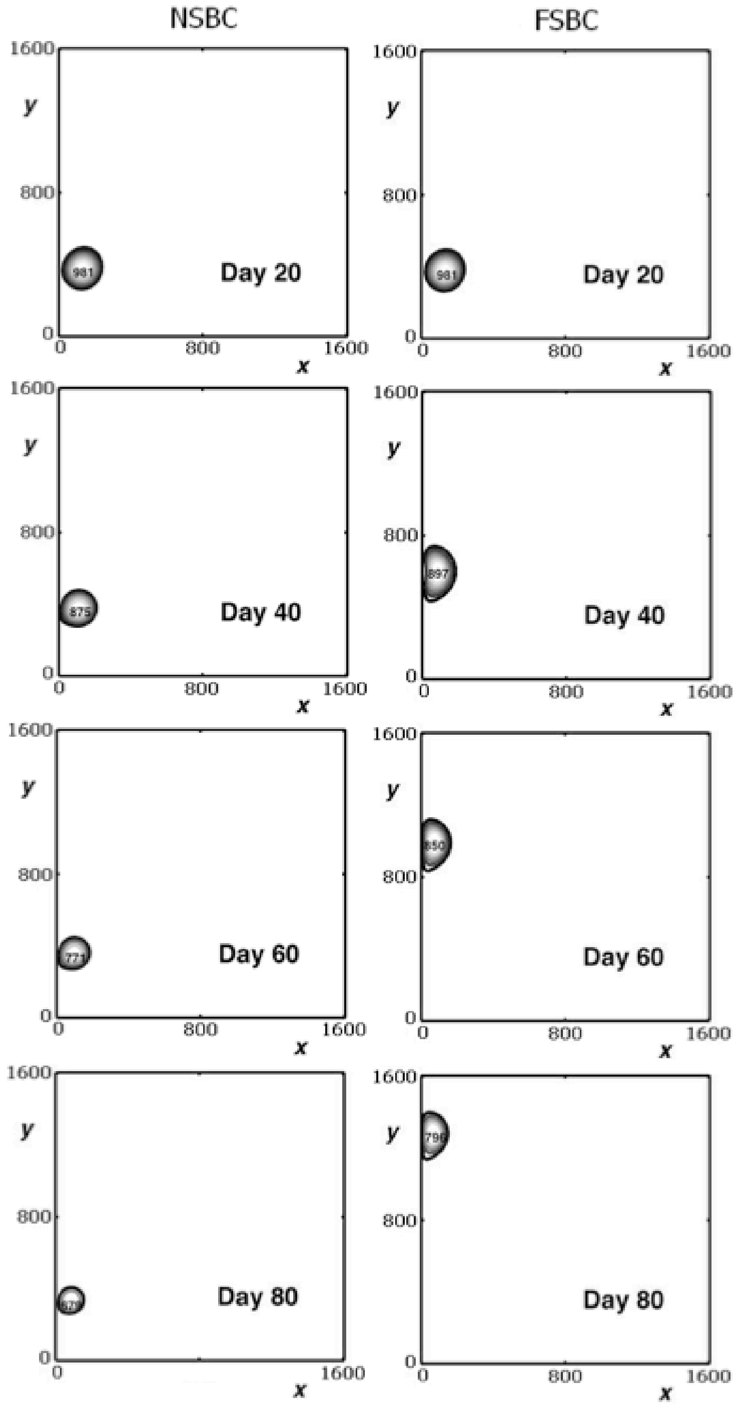

Figure 3. Evolution of an eddy encountering a meridional wall with NSBC (left panels) and FSBC (right panels). Parameters are $R = 100$ km, $H = 500$ m, $\beta = 2.3\times10^{-11}\,\mathrm{m}^{-1}\,\mathrm{s}^{-1}$, and $\alpha = 1$ initially. The scales on the coordinate axes are given in kilometers; the lines of constant upper-layer depth are spaced by 50 m, starting from 550 m. Maximal depth is given inside the eddy contours. The eddy begins movement when the distance between its center and the wall is 200 km.

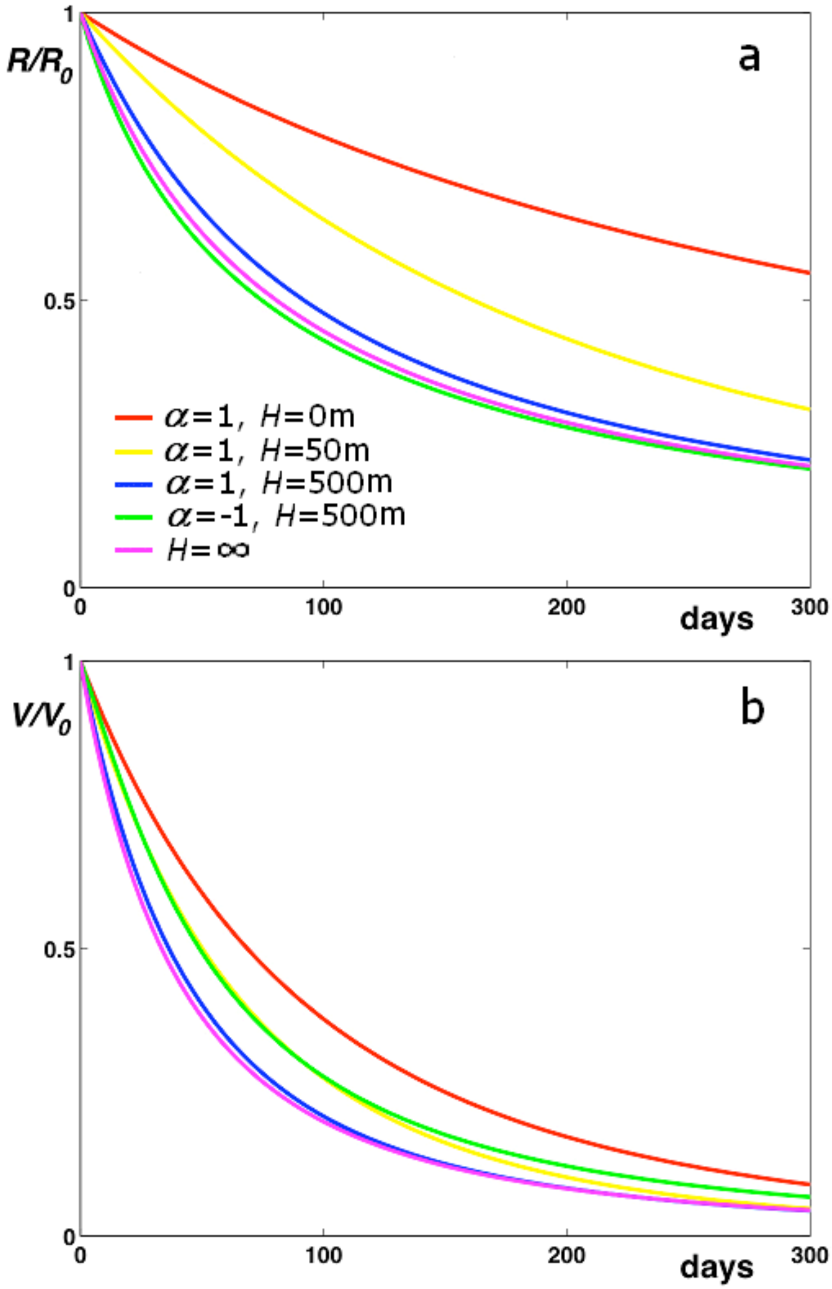

Figure 4. Decaying of eddies whose radii are 50 km and $\alpha = \pm 1$ initially: "lens" (red lines), anticyclonic eddy with $H = 50$ m (yellow lines), anticyclonic eddy with $H = 500$ m (blue lines), cyclonic eddy with $H = 500$ m (green lines), and cylindrical eddy in the limit of $H \to \infty$ (magenta lines). (a) Ratio R / R_0 versus time; (b) ratio V / V_0.

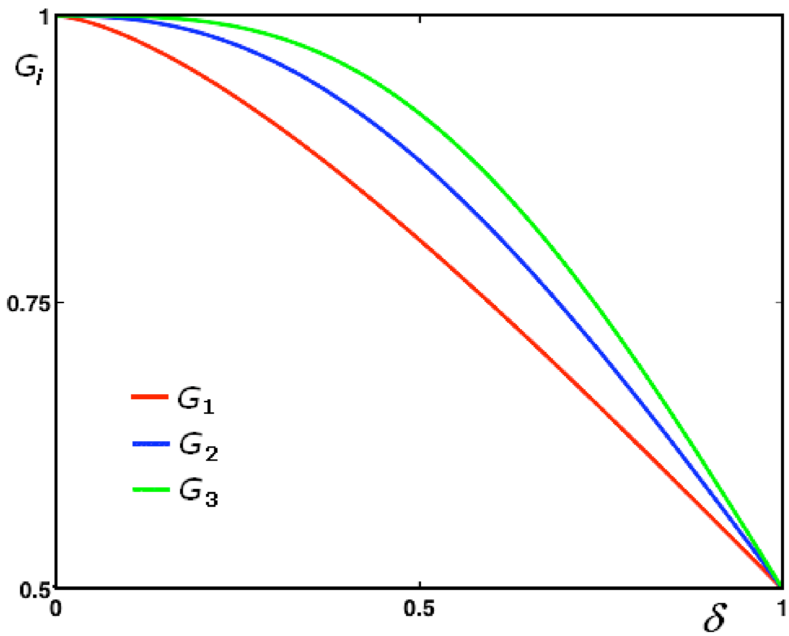

Figure 5. Dependence of $I_1 / \left(\pi R^2\right) = G_1(\delta)$ (red curve), $I_2 / \left(\pi R^4 / 2\right) = G_2(\delta)$ (blue curve), and $I_3 / \left(\pi R^6 / 3\right) = G_3(\delta)$ (green curve) on δ. Here $\delta = 0$ corresponds to the initial moment of the encounter (touching), $\delta = 1$ corresponds to complete transformation into a wodon.

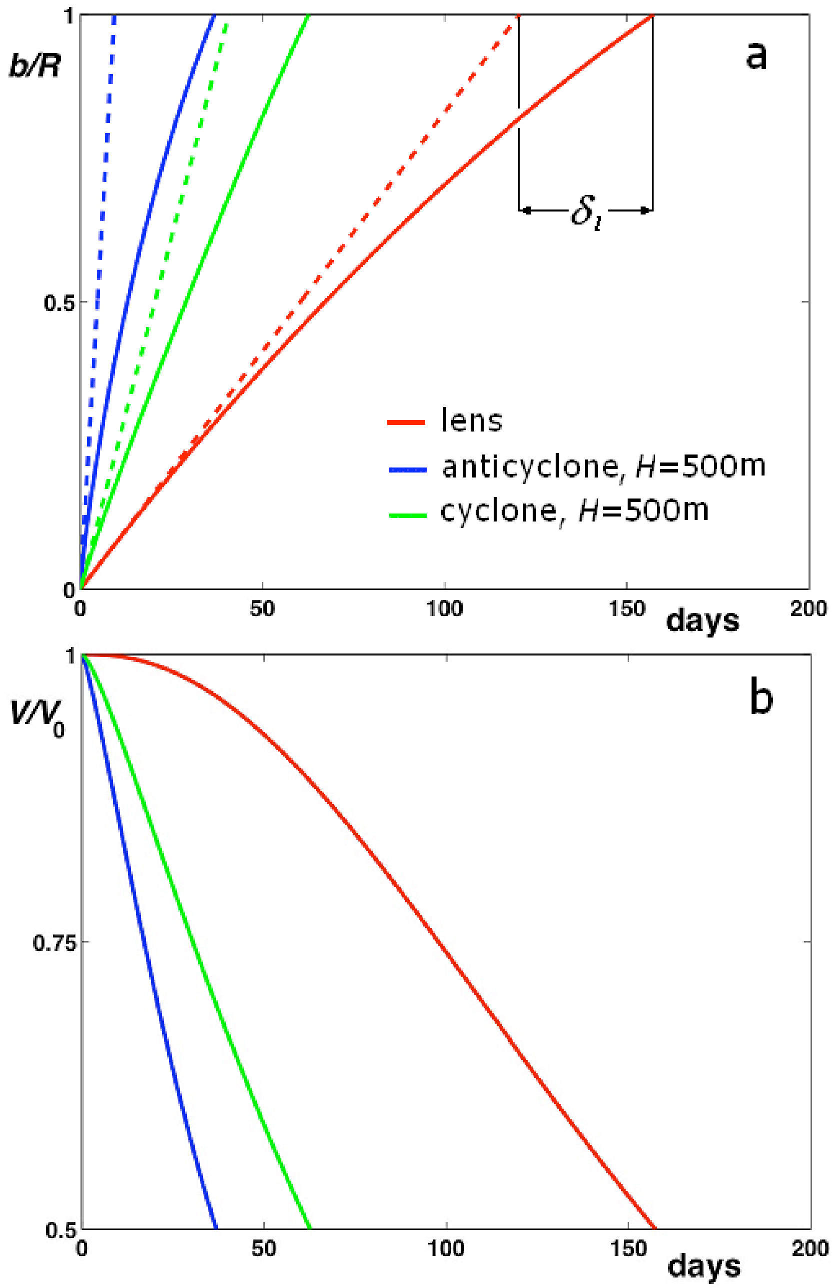

Figure 6. Idealized wodonization of eddies whose radii are 50 km: lens (red lines), anticyclonic eddy with $H = 500$ m (blue lines), and cyclonic eddy with $H = 500$ m (green lines). (a) Evolution of $\delta = b / R$ (solid lines). For comparison, the straight dashed lines show the movement of eddies in the open ocean (with constant speed C_{xi}). (b) Decrease in volume (V / V_0).

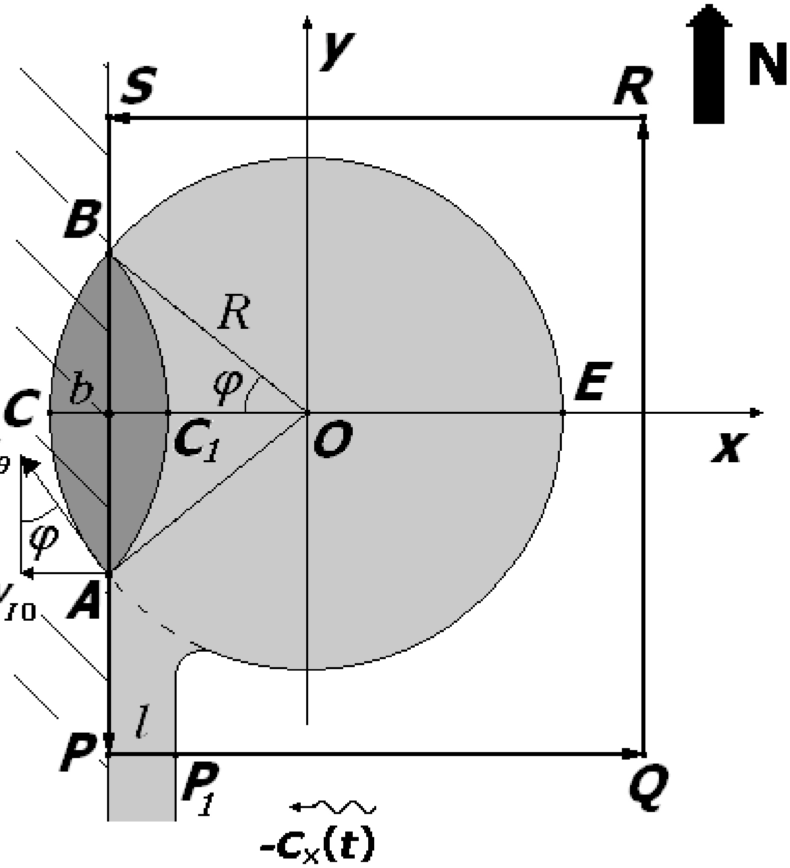

Figure 7. Schematic plot for the estimation of the image effect. The segment AC_1B is the mirror reflection of ACB. A projection of the orbital speed v_θ on the horizontal axis (v_{I0}) shows the imaginary "speed" of particles inside the segment ACB, which is blocked and "turned back" by the wall. According to the momentum conservation, we equate the ratio of this speed and the real velocity of the entire truncated eddy to the ratio of the volumes of the entire eddy and the segment ACB.

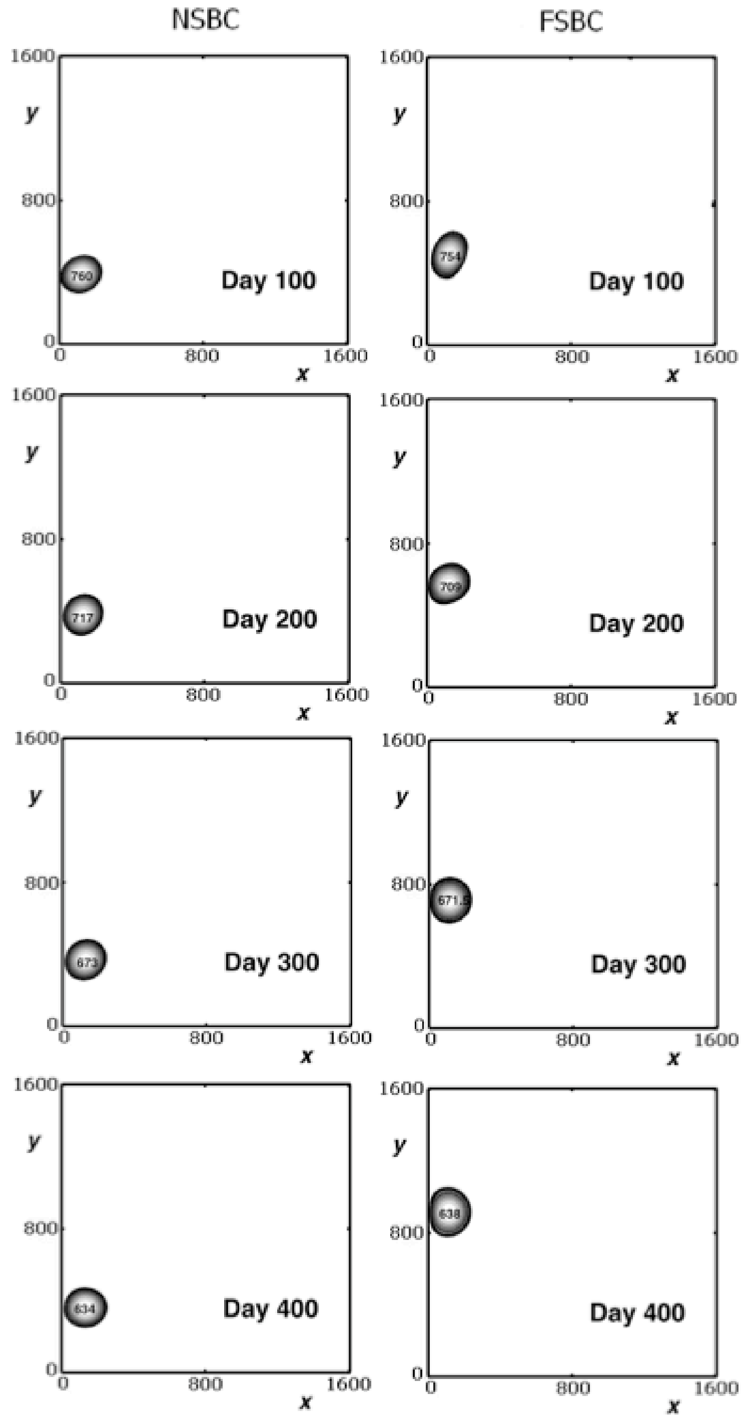

Figure 8. Evolution of an eddy tangent to a meridional wall on an f-plane with NSBC (left panels) and FSBC (right panel). Parameters are $R = 100$ km, $H = 300$ m, $\alpha = 1$ initially. The lines of constant upper-layer depth are uniformly spaced by 50 m, starting from 350 m.

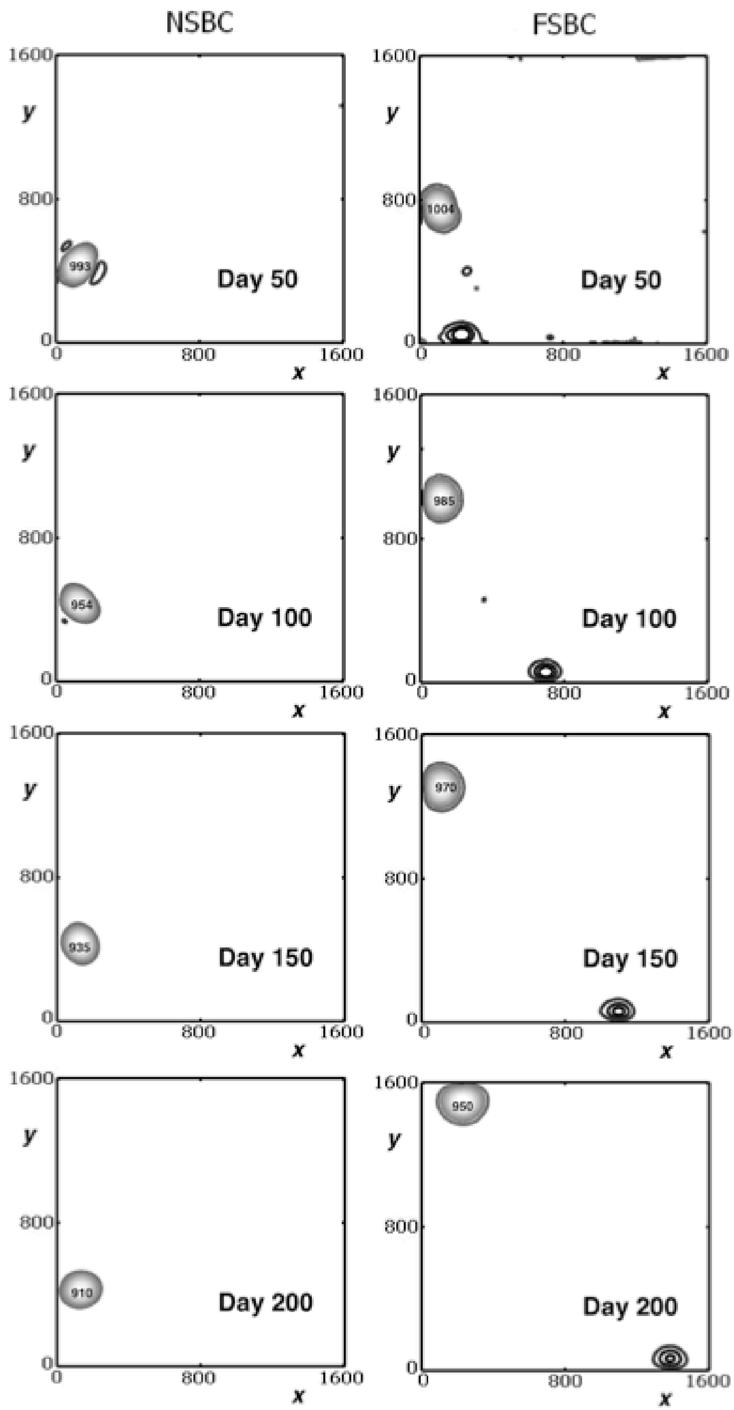

Figure 9. The same as in Figure 8 but for $H = 500$ m. The lines of constant upper-layer depth are spaced by 50 m, starting from 350 m but skipping 500 m. It is seen that the main eddy propagation speed is significantly larger than for $H = 300$ m, and companion cyclonic vortices appear.

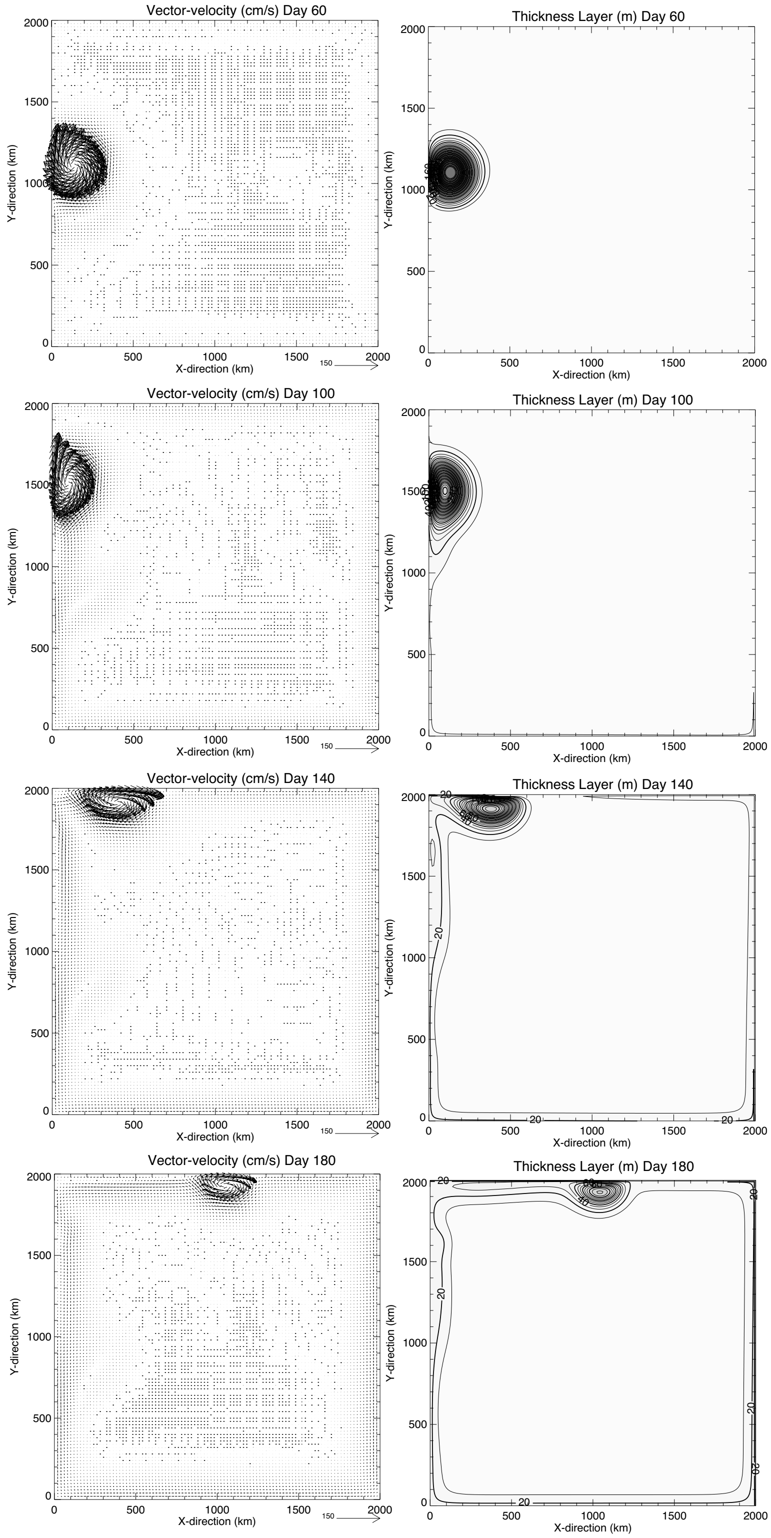

Figure 10. Evolution of an eddy with Gaussian orbital velocity structure tangent to a meridional wall on an *f*-plane, in the FSBC case. The snapshots are given for a 40-day period, starting with the 60th day. The left panel shows the vector-velocities of the eddy particles.